Progress In Electromagnetics Research C, Vol. 77, 91–100, 2017

Dual-Band Polarization-Insensitive Metamaterial Inspired Microwave Absorber for LTE-Band Applications

Kanwar P. Kaur[1, *], Trushit Upadhyaya[1], and Merih Palandöken[2]

Abstract—In this paper, the design, simulation and measurement of a dual-band polarization-insensitive metamaterial inspired microwave absorber are presented. The unit cell is composed of two concentric closed ring resonator (CRR) structures forming octagonal rings which are carved on an FR-4 dielectric substrate to give maximum absorption at dual frequencies of 2.09 GHz and 2.54 GHz. At these frequencies, the minimum reflection coefficients of −29.15 dB and −18.76 dB are achieved with absorption rates of 99.88% and 98.67% and narrow 10 dB bandwidths of 2.62% and 2.76%, respectively. Microwave absorption property of the proposed absorber structure is simulated by setting the perfect electric boundary conditions in four planes whose surface normal vectors are directed perpendicular to the wave propagation direction. These numerical computation settings replicate the rectangular waveguide to be used in the experimental measurements for the comparison between the simulated and experimental results. It is experimentally verified by the waveguide measurement method that the absorption rates about 99% are achieved for dual bands with polarization insensitivity thereby meeting the absorption requirements of LTE-band frequencies for a real time microwave absorber based energy harvesting systems.

1. INTRODUCTION

Electromagnetic (EM) metamaterials (MTMs) [1–3] are basically artificial or manmade materials. Recently, MTMs have gained wide attention in the field of research due to their unusual properties which are not available in naturally existing materials. The popularity of MTM arises from the fact that its properties can be altered by merely changing the geometrical parameters of a unit cell. The frequency selective surface (FSS) structures are normally designed in a periodic arrangement of unit cells, which have geometric sizes comparable to sub-wavelength. The sub-wavelength unit cells should have dimensions much less than the guided wavelength in the structure (λ), typically less than $\lambda/4$ [4] for MTMs to operate as natural materials. Some of the potential applications of MTMs include EM cloaking [5, 6], super lens [7, 8], antenna [9–11], bolometer [12], microwave absorbers [13–39] and energy harvesting system [40]. N. I. Landy in 2008 [13] has proposed the first MTM microwave absorber with simulated absorbance of 96% and experimental absorbance of 88% at 11.5 GHz frequency. MMAs are developed and studied for potential applications like sensors, radar cross section (RCS) reduction, medical imaging, spectroscopic detector and solar cell applications, to name a few. As a result of these magnificent properties, the MMAs are explored from single-band [14, 15], dual-band [16–18], triple-band [19–22], quad-band [23, 24] in the form of multi-band [25–27] up to narrow band [28, 29] and broad band [30, 31] with frequency ranging from microwaves [29, 30] to terahertz [32]. Any EM absorber performance is determined by how efficiently it absorbs the input EM signals. The key parameter which

Received 5 June 2017, Accepted 8 August 2017, Scheduled 26 August 2017

* Corresponding author: Kanwar Preet Kaur (kanwarpreet27@gmail.com).

[1] Department of Electronics & Communication Engineering, Chandubhai S. Patel Institute of Technology, Charotar University of Science & Technology, Changa, Anand, Gujarat, India. [2] Department of Electrical and Electronic Engineering, Izmir Katip Celebi University, Izmir, Turkey.

defines the optimum performance of an absorber is its absorption efficiency. According to the effective medium theory [33] the absorber efficiency is described by the equation [34]

$$A(\omega) = 1 - R(\omega) - T(\omega) \tag{1}$$

In the above equation, $A(\omega), R(\omega)$ and $T(\omega)$ represent the absorption coefficient, reflection coefficient and transmission coefficient, respectively. The reflection coefficient and transmission coefficient are related to the S-parameter by the following equations

$$\left.\begin{aligned} R(\omega) &= |S_{11}(\omega)|^2 \\ T(\omega) &= |S_{21}(\omega)|^2 \end{aligned}\right\} \tag{2}$$

where $S_{11}(\omega)$ is the return loss, and $S_{21}(\omega)$ is the insertion loss. A perfect metamaterial absorber (MMA) is one which has zero reflection coefficient and zero transmission coefficient. $T(\omega)$ can be reduced to zero by carving FSS on the top side of the dielectric substrate with a perfect electric conductor (PEC) at the backside. Whereas, by matching the input impedance of the structure to the free space impedance, $R(\omega)$ can be reduced to a minimum value (theoretically zero). In case of MMAs, the impedance matching is achieved by varying geometrical parameters of the unit cell, consequently altering the effective permittivity (ε) and permeability (μ) of the structure [34, 35].

Thus, aforementioned equation of absorber efficiency reduces to take the form of $A(\omega) = 1 - R(\omega)$. ($A(\omega) = 1$ — due to the impedance matching methods to be applied for the MTM absorber, the $R(\omega)$ is reduced to a value very near to zero, which results $A(\omega)$ to be effectively 1 — total absorption). As the MMA surface, composed of MTM unit cells, can be considered as an effectively homogeneous medium hence the S-parameters of a MMA can be related to an effective refractive index ($n_{\text{eff}}(\omega)$) and effective normalized impedance ($z_{\text{eff}}(\omega)$) [36].

In this paper, the design, simulation and experimental demonstration based on waveguide measurement method are presented for a dual-band polarization-insensitive MTM inspired microwave absorber. The proposed absorber structure consists of two concentric rings exhibiting dual absorption maxima at S-band frequencies. The design is simulated using 3D full wave commercial electromagnetic field solver, HFSS (High Frequency Structure Simulator) software. PEC boundary conditions are set in all four surfaces whose surface normal vectors are directed perpendicular to the wave propagation direction to replicate the side surfaces of practical waveguide component, which has been utilized in the experimental measurement setup. These boundary conditions are selected to have better scientific comparison between the numerical and experimental results. The polarization independence/insensitivity feature is tested numerically and experimentally with small number of unit cells in a reduced MMA geometrical size by setting different orientations of the concentric CRRs, which is the main reason why to use this method for the effective MMA characterization. In this study, different samples for various CRR orientations are fabricated and each sample is tested for the polarization insensitivity by measuring return loss for each sample. The effectiveness of the proposed MMA has been explored through the simulated results of $S_{11}(\omega)$, $z_{\text{eff}}(\omega)$, electric field and surface current distributions in addition to the polarization variations. The simulation results show that the two absorption maxima of 99.88% and 98.67% are obtained at 2.09 GHz and 2.54 GHz, respectively, thereby covering frequencies of LTE band. Hence, the proposed dual-band absorber can be used in for absorbing ambient LTE frequencies, which improves the EMI/EMC immunity of the high speed RF electronic components operating in wireless environments separated from the RF sources in short distances. The paper is organized as follows. Details of the proposed dual-band MMA design are presented in Section 2. In Section 3, the simulated results for various geometric parameters are discussed. Section 4 presents the fundamental theory of how the propagating EM energy is absorbed, followed by the experimental setup and the results with the comparative plots in Section 5. Concluding remarks are conducted in Section 6.

2. METAMATERIAL ABSORBER DESIGN PRINCIPLE

The proposed MMA design with its optimized geometrical dimensions is shown in Fig. 1. The unit cell is made up of two concentric octagonal rings forming CRRs. Outer CRR results in the first lower frequency absorption maxima whereas inner CRR gives rise to the second higher frequency absorption

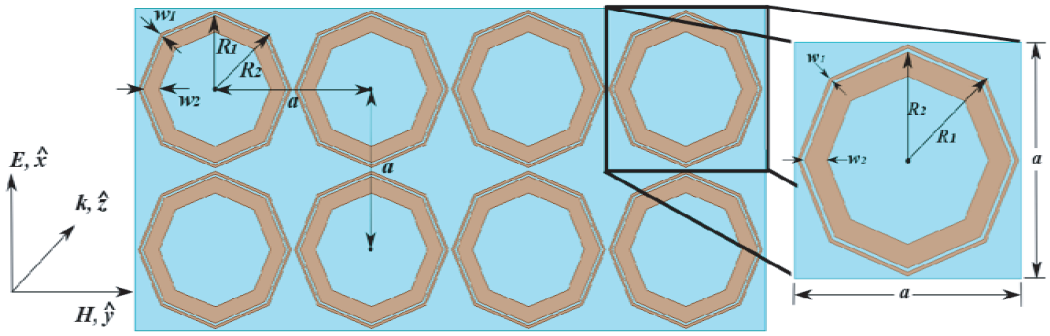

Figure 1. Proposed absorber structure geometries with concentric octagonal rings: Front view of an optimized sample and a single unit cell.

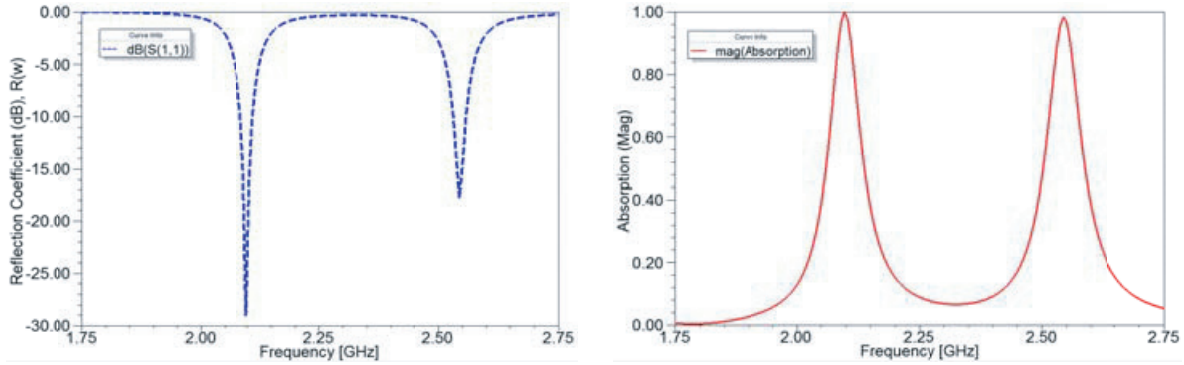

(a) (b)

Figure 2. Simulated results of proposed absorber structure under normal incidence: (a) Reflection Coefficient, $S_{11}(\omega)$ and (b) Absorption, $A(\omega)$.

peak. These concentric CRRs are engraved on a double-sided metalized FR-4 dielectric substrate of 2.4 mm thickness. The copper layer has the conductivity of 5.8×10^7 S/m and thickness of 0.035 mm. The relative permittivity of FR4 is 4.4 with the dielectric loss tangent of 0.02. The optimized geometrical dimensions of the proposed structure are as follows: $a = 27.4$ mm, $R_1 = 13.4$ mm, $R_2 = 12.52$ mm, $w_1 = 0.44$ mm and $w_2 = 2.8$ mm. The final MMA has the thickness of approximately $\lambda/58$ and maximum lateral size less than $\lambda/5$ at low frequency resonance.

3. NUMERICAL COMPUTATION RESULTS

For numerical simulations, an array of 2×4 unit cells with the periodicity of $a = 27.4$ mm is selected. The absorber structure with single unit cell is configured to an optimized array structure to achieve dual-band absorption with high absorption rate. This structure is simulated using PEC boundary conditions with normal incidence of EM wave on the MMA. No transmission is possible through the absorber structure since PEC is appended at the backplane of the absorber. Thus, to achieve maximum absorption the only parameter which is to be minimized is the reflection coefficient. This reflection coefficient minimization is done by altering the geometrical parameters of the absorber structure thereby matching the structure impedance to the free space impedance. The simulated reflection coefficient and corresponding absorption efficiency are depicted in Fig. 2. The plot of $S_{11}(\omega)$, Fig. 2(a), shows two distinct minima of -29.15 dB and -18.76 dB with the absorption efficiency, determined from Eq. (1), of 99.88% and 98.67% at lower S-band frequencies of 2.09 GHz and 2.54 GHz, respectively. The corresponding absorption plot is shown in Fig. 2(b). Hence this dual-band absorber can be used in the MMA based energy harvester systems for the absorption of ambient LTE band frequencies to be harvested. A comparative graph that depicts absorption and reflection is shown in Fig. 3(a). To

achieve the desired condition of impedance matching the structure is optimized such that the impedance of the MMA structure roughly matches to the free space impedance where the real component of normalized $z_{\text{eff}}(\omega)$ is nearly equal to unity whereas imaginary component approaches to zero. The retrieved impedance, illustrated in Fig. 3(b), shows that the two impedances roughly match at the frequencies where $z'_{eff}(\omega) \approx 1$ (real component) and $z''_{eff}(\omega) \approx 0$ (imaginary component).

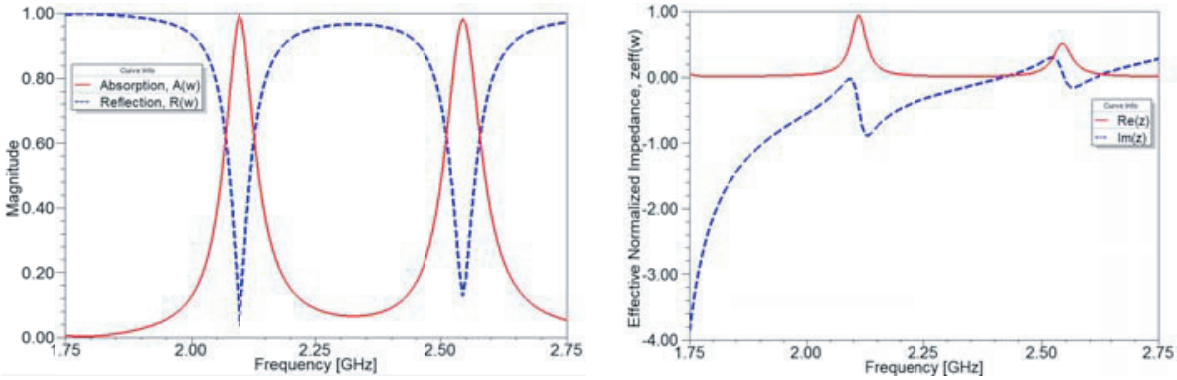

(a) (b)

Figure 3. (a) Comparative graphs depicting absorption, $A(\omega)$ and reflection, $R(\omega)$ and (b) effective normalized impedance, $z_{\text{eff}}(\omega)$.

In the numerical calculations, the polarization angle (ϕ) and oblique angle (θ) dependences of the structure cannot be obtained directly by changing the ϕ and θ angles in numerical computation due to setting of the wave polarization and incidence angles by H_{10} fundamental mode of the rectangular waveguide. However, the polarization insensitivity of the structure, depicted in Fig. 4, is obtained by setting different orientation angles for the concentric octagonal rings.

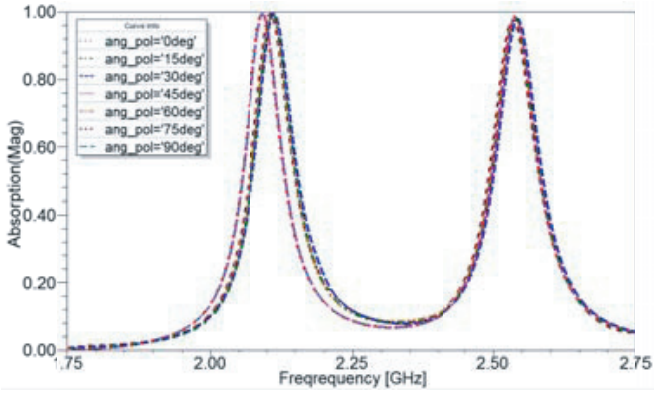

Figure 4. Simulated absorption coefficient for different FSS orientation replicating polarization angle variation.

4. METAMATERIAL ABSORBER OPERATION PRINCIPLE

For comprehending the fundamental physics behind the absorption in MMA, the numerically calculated electric field distribution and surface current distribution for CRRs at dual absorbing frequencies are shown in Figs. 5 and 6. From Fig. 5, it is seen that the normal incidence of the EM wave on MMA increases the electric field component which is concentrated strongly along the outer octagonal ring at lower absorption frequency. At higher absorption frequency band, the major field concentration is

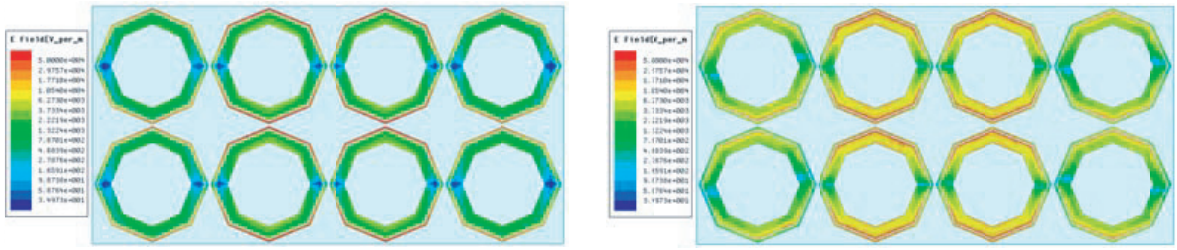

(a) (b)

Figure 5. Numerically calculated induced electric field distributions, (a) lower absorption frequency (b) at higher absorption frequency.

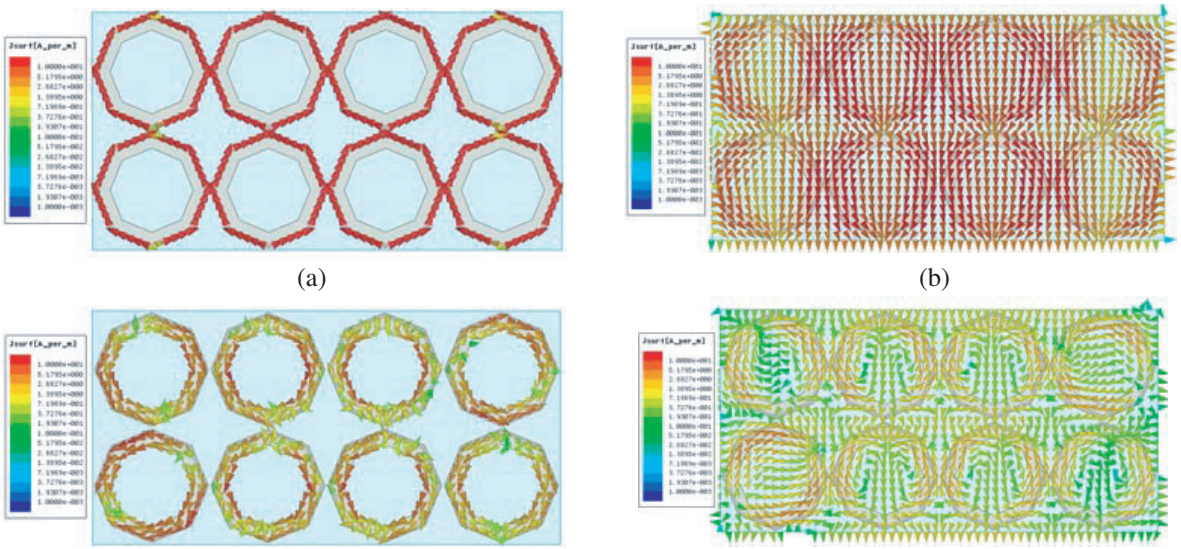

(a) (b)

(c) (d)

Figure 6. Numerically calculated surface current distribution for the CRRs and ground plane: (a) and (b) Surface current distribution at lower absorption frequency for CRRs and ground plane. (c) and (d) Surface current distribution at higher absorption frequency CRRs and ground plane.

along the edges of the inner ring. Thus the electric field distribution of the unit cells is affected by the incident EM wave and MMA geometry which in turn influences the effective material parameters of the structure.

The surface current distributions on the top and bottom sides for lower and higher absorption frequencies are shown in Fig. 6. It is apparent that for the incident EM wave, an antiparallel current is generated between CRR and the ground plane, and also between the two octagonal rings. This antiparallel current generates a circulating current loop perpendicular to the incident magnetic field leading to magnetic response. This magnetic response in turn affects the effective permeability ($\mu_{\text{eff}}(\omega)$) of the structure. Thus, by individually controlling the electric and magnetic response, a frequency condition can be achieved where the impedance of the MMA matches to the free space impedance. The 10 dB bandwidths for the dual bands are obtained as 2.62% and 2.76% for the lower and higher absorption maxima, respectively. As seen from the numerical results, a very narrow band of absorption is obtained at the resonant frequencies. This narrow band can be improved either by appending one or more FSS layers or by forming multiple resonances at close frequencies.

The proposed absorber is also studied for the variation in loss tangent of the substrate up to 100% as shown in Fig. 7. It is observed that the increase in loss tangent will increase the substrate loss subsequently causing imaginary part of the wave impedance to be increased with the result of degradation in the absorption process. The geometric parameters are therefore needed to be adjusted

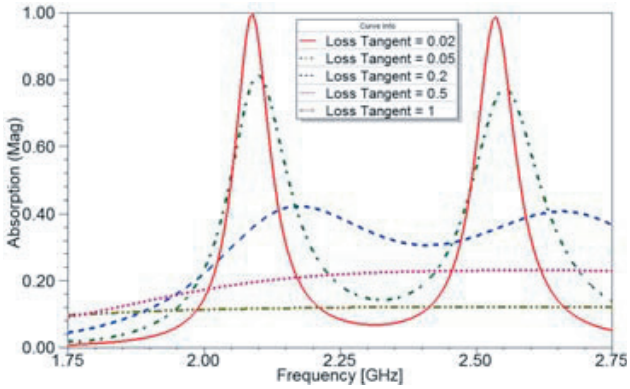

Figure 7. Simulated absorption coefficient for various loss tangents.

Table 1. Comparison of various microwave MMAs.

Reference Article	Number of Absorption Bands	Absorption (%)	Absorption Frequencies (GHz)	Cell Size (mm)
[16]	Dual	95.6, 99.9	4.32, 5.73	19.9
[17]	Dual	99.8, 99.97	5.5, 8.9	10
[20]	Triple	99.9, 97.9, 97.8	4.84, 8.06, 11.28	14
[21]	Triple	66.88, 98.06, 99.97	4.97, 11.27, 13.43	10
[26]	Multi (Quad)	98.81, 99.68, 99.98, 99.34	4.11, 7.91, 10.13, 11.51	15
[29]	Dual	98.1, 99	7, 10.7	4×7.2
Proposed MMA	Dual	99.88, 98.67	2.09, 2.54	27.4

to have better absorption at the specified frequencies with the inherent effect of increased absorption bandwidth. Furthermore, Table 1 presents the comparison of absorption, respective frequencies, and cell size of the proposed MMA absorber with the previously published microwave MMAs. Table 1 shows the novelty in frequency selection so that the proposed dual-band absorber can be practically utilized for improving the EMI/EMC immunity of the high speed RF electronic components by absorbing ambient LTE frequencies.

5. EXPERIMENTAL RESULTS

From the polarization angle variation graph depicted in Fig. 4, it can be concluded that the absorption rate is independent of the ϕ variation in the first absorption band for 0°, 45° and 90° angles. For the rest of ϕ angles, the absorption rate is also polarization independent with slight frequency shift. Thus, for the practical examination of polarization insensitivity of the proposed structure, one sample from each set of angles is selected. Finally, MMA unit cell with the orientation angles of 0° and 30° are chosen for the fabrication using standard printed circuit board (PCB) techniques. The two fabricated samples are shown in Fig. 8. Sample-1 corresponds to the actual sample without any orientation whereas Sample-2 corresponds to the samples with 30° inclination angle with respect to the Sample-1. These samples are tested using waveguide measurement technique [37–39] instead of free-space measurement system [13–15]. As the latter technique requires sample size in the order of 10λ, which results in comparatively large size samples of proposed absorber to be tested. Sample size in case of waveguide measurement technique is the same as that of the inner aperture dimension of the WR-430 waveguide. In this method, the sample and a copper sheet of same size are placed at center of the waveguide and connected by

means of Teflon coated RG142 coaxial cable to an Agilent N9912A vector network analyzer (VNA). The waveguide setup is terminated with a metal plate to block propagating EM waves as in the case of metallic backside of MMA. The complete measurement setup is depicted in Fig. 8(c).

The experimental results of the return loss and corresponding absorption coefficient for Sample-1 are illustrated in Fig. 9. Good agreement between the simulated and measured results can be observed clearly from Fig. 9. Fig. 10 shows the experimental results of Sample-2 replicating the variation in the polarization angle (ϕ). Simulated absorption efficiency is compared with the measured absorption efficiency of Sample-1 and Sample-2. They are depicted in Fig. 11. It can be observed that the measured absorption efficiencies of Sample-1 and Sample-2 fairly match to the respective simulated absorption efficiencies with slight frequency shift. The main reason behind the closeness of the results is due to the folding symmetry exhibited by proposed MMA design. However, the waveguide section in the experimental setup can be extended with an additional waveguide transmission line section to get rid of the small ripples existing in Fig. 11. Thus, it is experimentally verified that the proposed MMA is insensitive to the polarization of the incident EM waves. Slight deviation between the simulated and experimental results is mainly due to the fabrication tolerance and the imperfection in dielectric substrate.

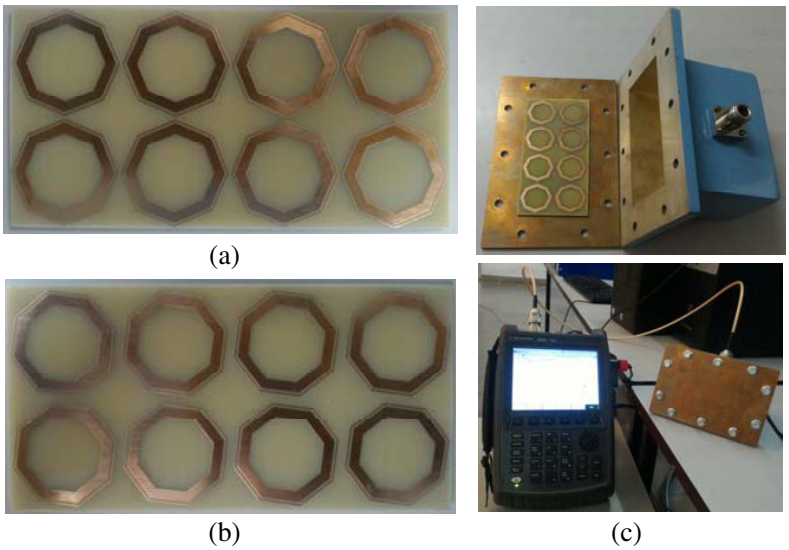

Figure 8. Photograph of the fabricated samples. (a) Sample-1. (b) Sample-2. (c) Photograph of the test setup of waveguide measurement method.

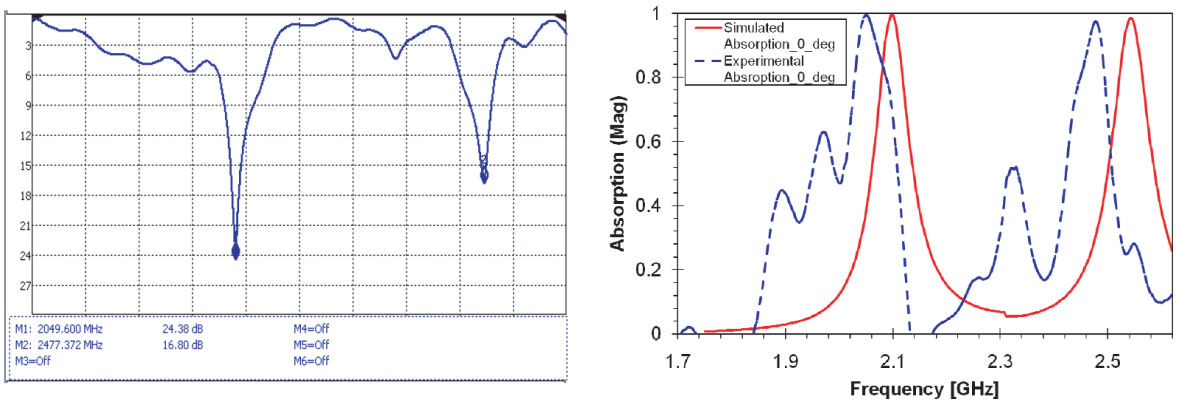

Figure 9. Photographs of Experimental Results for Sample-1. (a) Return loss. (b) Comparative absorption graph.

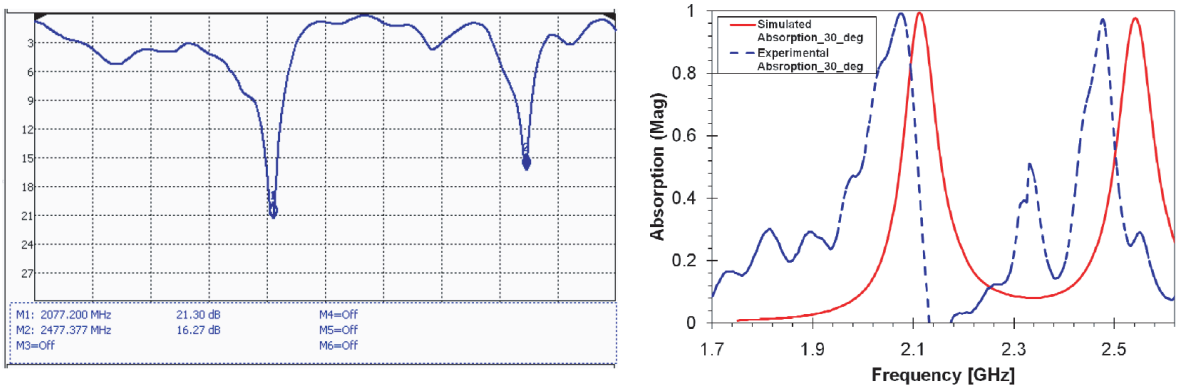

Figure 10. Photographs of experimental results for Sample-2. (a) Return loss. (b) Comparative absorption graph.

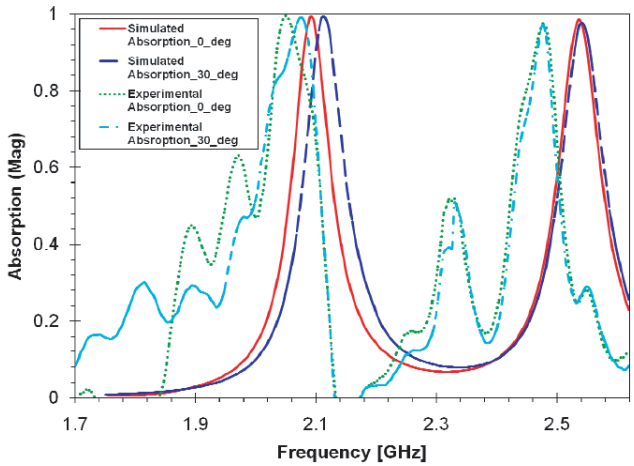

Figure 11. Comparative absorption graph depicting simulated and measured absorption efficiency.

6. CONCLUSIONS

A dual-band microwave metamaterial absorber composed of two concentric octagonal CRRs engraved on an FR-4 dielectric substrate is presented in this paper. The proposed dual-band absorber has two distinct absorption peaks of 99.88% and 98.67% at S-band frequencies of 2.09 GHz and 2.54 GHz. The absorber can be used as a primary component in the energy harvester modules for the absorption of specifically LTE-band frequencies. In numerical calculations, the imposed boundary conditions are selected to replicate the practical waveguide measurement setup to verify the dual-band absorption feature of the proposed MMA. The numerical and measured results have good agreement. For the practical determination of polarization independence of the proposed absorber, two samples with different unit cell orientations are fabricated and tested with a good agreement between simulated and measured results.

REFERENCES

1. Veselago, V. G., "The electrodynamics of substances with simultaneously negative values of ε and μ, *Soviet Physics Uspekhi*, Vol. 10, No. 4, 509, 1968.
2. Smith, D. R., J. B. Pendry, and M. C. Wiltshire, "Metamaterials and negative refractive index," *Science*, Vol. 305, No. 5685, 788–792, Aug. 6, 2004.

3. Smith, D. R., W. J. Padilla, D. C. Vier, S. C. Nemat-Nasser, and S. Schultz, "Composite medium with simultaneously negative permeability and permittivity," *Physical Review Letters*, Vol. 84, No. 18, 4184, May 1, 2000.
4. Caloz, C. and T. Itoh, *Electromagnetic Metamaterials: Transmission Line Theory and Microwave Applications*, John Wiley & Sons, Nov. 2005, 22.
5. Schurig, D., J. J. Mock, B. J. Justice, S. A. Cummer, J. B. Pendry, A. F. Starr, and D. R. Smith, "Metamaterial electromagnetic cloak at microwave frequencies," *Science*, Vol. 314, No. 5801, 977–980, Nov. 10, 2006.
6. Cai, W., U. K. Chettiar, A. V. Kildishev, and V. M. Shalaev, "Optical cloaking with metamaterials," *Nature Photonics*, Vol. 1, No. 4, 224–227, Apr. 1, 2007.
7. Pendry, J. B., "Negative refraction makes a perfect lens," *Physical Review Letters*, Vol. 85, No. 18, 3966, Oct. 30, 2000.
8. Fang, N. and X. Zhang, "Imaging properties of a metamaterial superlens," *Applied Physics Letters*, Vol. 82, No. 2, 161–163, Jan. 13, 2003.
9. Upadhyaya, T. K., S. P. Kosta, R. Jyoti, and M. Palandöken, "Novel stacked μ-negative material-loaded antenna for satellite applications," *International Journal of Microwave and Wireless Technologies*, Vol. 8, No. 02, 229–235, Mar. 1, 2016.
10. Upadhyaya, T. K., S. P. Kosta, R. Jyoti, and M. Palandöken, "Negative refractive index material-inspired 90-deg electrically tilted ultra-wideband resonator," *Optical Engineering*, Vol. 53, No. 10, 107104, Oct. 1, 2014.
11. Palandöken, M., *Artificial Materials Based Microstrip Antenna Design*, INTECH Open Access Publisher, 2011.
12. Niesler, F. B., J. K. Gansel, S. Fischbach, and M. Wegener, "Metamaterial metal-based bolometers," *Applied Physics Letters*, Vol. 100, No. 20, 203508, May 14, 2012.
13. Landy, N. I., S. Sajuyigbe, J. J. Mock, D. R. Smith, and W. J. Padilla, "Perfect metamaterial absorber," *Physical Review Letters*, Vol. 100, No. 20, 207402, May 21, 2008.
14. Zhu, B., Z. Wang, C. Huang, Y. Feng, J. Zhao, and T. Jiang, "Polarization insensitive metamaterial absorber with wide incident angle," *Progress In Electromagnetics Research*, Vol. 101, 231–239, 2010.
15. Cheng, Y. and H. Yang, "Design, simulation, and measurement of metamaterial absorber," *Journal of Applied Physics*, Vol. 108, No. 3, 034906, Aug. 1, 2010.
16. Dincer, F., M. Karaaslan, E. Unal, K. Delihacioglu, and C. Sabah, "Design of polarization and incident angle insensitive dual-band metamaterial absorber based on isotropic resonators, *Progress In Electromagnetics Research*, Vol. 144, 123–132, 2014.
17. Ramya, S. and I. Srinivasa Rao, "Design of polarization-insensitive dual band metamaterial absorber," *Progress In Electromagnetics Research M*, Vol. 50, 23–31, 2016.
18. He, X. J., Y. Wang, J. Wang, T. Gui, and Q. Wu, "Dual-band terahertz metamaterial absorber with polarization insensitivity and wide incident angle," *Progress In Electromagnetics Research*, Vol. 115, 381-397, 2011.
19. Shen, X., Y. Yang, Y. Zang, J. Gu, J. Han, W. Zhang, and T. J. Cui, "Triple-band terahertz metamaterial absorber: Design, experiment, and physical interpretation," *Applied Physics Letters*, Vol. 101 No. 15, 154102, Oct. 8, 2012.
20. Wang, G. D., J. F. Chen, X. Hu, Z. Q. Chen, and M. Liu, "Polarization-insensitive triple-band microwave metamaterial absorber based on rotated square rings," *Progress In Electromagnetics Research*, Vol. 145, 175–183, 2014.
21. Sood, D., "A triple band ultra-thin metamaterial absorber with wide incident angle stability," *Indian Journal of Radio & Space Physics (IJRSP)*, Vol. 45, No. 2, 57–66, Dec. 29, 2016.
22. Yahiaoui, R., J. P. Guillet, F. de Miollis, and P. Mounaix, "Ultra-flexible multiband terahertz metamaterial absorber for conformal geometry applications," *Optics Letters*, Vol. 38, No. 23, 4988–4990, 2013.
23. Agarwal, M., A. K. Behera, and M. K. Meshram, "Wide-angle quad-band polarization-insensitive metamaterial absorber," *Electronics Letters*, Vol. 52, No. 5, 340–342, Jan. 22, 2016.

24. Wang, N., J. Tong, W. Zhou, W. Jiang, J. Li, X. Dong, and S. Hu, "Novel quadruple-band microwave metamaterial absorber," *IEEE Photonics Journal*, Vol. 7, No. 1, 1–6, Feb. 2015.
25. Park, J. W., P. V. Tuong, J. Y. Rhee, K. W. Kim, W. H. Jang, E. H. Choi, L. Y. Chen, and Y. Lee, "Multi-band metamaterial absorber based on the arrangement of donut-type resonators," *Optics Express*, Vol. 21, No. 8, 9691–9702, Apr. 22, 2013.
26. Chaurasiya, D., S. Ghosh, S. Bhattacharyya, A. Bhattacharya, and K. V. Srivastava, "Compact multi-band polarization-insensitive metamaterial absorber," *IET Microwaves, Antennas & Propagation*, Vol. 10, No. 1, 94–101, Jan. 9, 2016.
27. Yahiaoui, R., S. Tan, L. Cong, R. Singh, F. Yan, and W. Zhang, "Multispectral terahertz sensing with highly flexible ultrathin metamaterial absorber," *Journal of Applied Physics*, Vol. 118, No. 8, 083103, 2015.
28. Huang, Y. J., G. J. Wen, J. Li, W. R. Zhu, P. Wang, and Y. H. Sun, "Wide-angle and polarization-independent metamaterial absorber based on snowflake-shaped configuration," *Journal of Electromagnetic Waves and Applications*, Vol. 27, No. 5, 552–559, Mar. 1, 2013.
29. Ramya, S. and I. Srinivasa Rao, "Dual band microwave metamaterial absorber using loop resonator for electromagnetic interference suppression," *Int. J. Appl. Eng. Res.*, Vol. 10, No. 30, 22712-22715, 2015.
30. Ding, F., Y. Cui, X. Ge, Y. Jin, and S. He, "Ultra-broadband microwave metamaterial absorber," *Applied Physics Letters*, Vol. 100, No. 10, 103506, Mar. 5, 2012.
31. Liu, Y., S. Gu, C. Luo, and X. Zhao, "Ultra-thin broadband metamaterial absorber," *Applied Physics A*, Vol. 108, No. 1, 19–24, Jul. 1, 2012.
32. Yahiaoui, R., K. Hanai, K. Takano, T. Nishida, F. Miyamaru, M. Nakajima, and M. Hangyo, "Trapping waves with terahertz metamaterial absorber based on isotropic Mie resonators," *Optics Letters*, Vol. 40, No. 13, 3197–3200, 2015.
33. Liu, R., T. J. Cui, D. Huang, B. Zhao, and D. R. Smith, "Description and explanation of electromagnetic behaviors in artificial metamaterials based on effective medium theory," *Physical Review E*, Vol. 76, No. 2, 026606, Aug. 23, 2007.
34. Tao, H., N. I. Landy, C. M. Bingham, X. Zhang, R. D. Averitt, and W. J. Padilla, "A metamaterial absorber for the terahertz regime: Design, fabrication and characterization," *Optics Express*, Vol. 16, No. 10, 7181–7188, May 12, 2008.
35. Tao, H., C. M. Bingham, A. C. Strikwerda, D. Pilon, D. Shrekenhamer, N. I. Landy, K. Fan, X. Zhang, W. J. Padilla, and R. D. Averitt, "Highly flexible wide angle of incidence terahertz metamaterial absorber: Design, fabrication, and characterization," *Physical Review B*, Vol. 78, No. 24, 241103, Dec. 19, 2008.
36. Smith, D. R., D. C. Vier, T. Koschny, and C. M. Soukoulis, "Electromagnetic parameter retrieval from inhomogeneous metamaterials," *Physical Review E*, Mar. 22, 2005, Vol. 71, No. 3, 036617.
37. Li, L., Y. Yang, and C. Liang, "A wide-angle polarization-insensitive ultra-thin metamaterial absorber with three resonant modes," *Journal of Applied Physics*, Sep. 15, 2011, Vol. 110, No. 6, 063702.
38. Lu, L., S. Qu, H. Ma, F. Yu, S. Xia, Z. Xu, and P. Bai, "A polarization-independent wide-angle dual directional absorption metamaterial absorber," *Progress In Electromagnetics Research M*, Vol. 27, 91–201, 2012.
39. Zhai, H., C. Zhan, L. Liu, and Y. Zang, "Reconfigurable wideband metamaterial absorber with wide angle and polarisation stability," *Electronics Letters*, Vol. 51, No. 21, 1624–1626, Oct. 1, 2015.
40. Palandöken, M., "Microstrip antenna with compact anti-spiral slot resonator for 2.4 GHz energy harvesting applications," *Microwave and Optical Technology Letters*, Vol. 58, No. 6, 1404–1408, 2016.